Geophysical Research Letters®

Key Points:

- Convection-permitting models can capture the response of Mesoscale Convective Systems to both moisture and shear in West Africa
- Strong shear gives larger cores, reduced entrainment and greater maximum and mean storm rainfall; this is missed in a parameterized model
- Shear response has upscale impacts through control of zonal distribution of biases in storm mean rainfall and diabatic heating

Wind Shear Effects in Convection–Permitting Models Influence MCS Rainfall and Forcing of Tropical Circulation

Ben Maybee[1] [ID], John H. Marsham[1] [ID], Cornelia M. Klein[2] [ID], Douglas J. Parker[1,3,4] [ID], Emma J. Barton[2,5] [ID], Christopher M. Taylor[2,5] [ID], Huw Lewis[6] [ID], Claudio Sanchez[6], Richard W. Jones[6] [ID], and James Warner[6] [ID]

[1]Institute for Climate and Atmospheric Science, University of Leeds, Leeds, UK, [2]UK Centre for Ecology and Hydrology, Wallingford, UK, [3]National Centre for Atmospheric Science, University of Leeds, Leeds, UK, [4]NORCE Norwegian Research Centre AS, Bjerknes Center for Climate Research, Bergen, Norway, [5]National Centre for Earth Observation, Wallingford, UK, [6]Met Office, Exeter, UK

Abstract Mesoscale Convective Systems (MCSs) play a critical role in tropical rainfall patterns and circulations. To reduce persistent biases and improve understanding of the climate system, international groups have called for unprecedented investment in global convection–permitting (CP) climate models. It is essential such models accurately represent MCSs, and in particular environmental interactions such as dynamical control by wind shear. We show that in representative current generation CP simulations, MCS updraft entrainment decreases with shear, leading to a realistic increase of extreme rainfall. We find the control of environmental shear extends to mean storm rainfall and anvil heights. The simulation of these effects depends strongly on model physics in both CP and parameterized models. We show that in West Africa, MCS shear response influences the zonal distribution of storm diabatic heating, modifying upscale impacts of convection. Our results demonstrate key tests for focused process–based assessment of CP model fidelity.

Plain Language Summary Movements of tropical air are driven by interactions between large, continental–scale circulations and localized deep convection — cells of ascending moist air reaching to the tropopause. These cells can aggregate to form Mesoscale Convective Systems (MCSs), long–lived thunderstorm clusters with large cold cloud shields that dominate tropical rainfall and atmospheric heating, forcing air circulations. Meanwhile, the strength of MCS rainfall depends on local atmospheric conditions. Such local process interactions occur on scales much smaller than typical global climate model grid spacings (>25 km), thus requiring a sub–grid parameterization of deep convection that introduces model biases. Here we show that kilometer–scale models can realistically capture the response of MCSs to local atmospheric moisture and wind conditions. A realistic response to the wind field relies on models showing variable mixing of dry environmental air into convective updrafts, with reduced rates for stronger vertical wind shear. We find that this wind (i.e., dynamical) control on MCSs explains patterns of mean rainfall biases in West Africa and influences atmospheric heating, likely mediating MCSs' upscale impacts on tropical circulations. Our results provide vital process–based methods for verifying the added value of explicitly representing convective storms in novel kilometer–scale global models.

1. Introduction

Deep moist convection dominates the tropical atmosphere. Up to 75% of tropical rainfall is attributed to convective storms (Feng et al., 2023; Roca et al., 2014). Yielding strong latent heat release from storm rainfall (C. Schumacher & Houze, 2003), significantly enhanced vertical transport (Chen et al., 2022), and interactions with synoptic–scale radiation budgets (Bony et al., 2020), organized deep convection is a critical component of tropical circulations (Bony et al., 2015; Tomassini & Yang, 2022). Exemplars of such organisation are Mesoscale Convective Systems (MCSs): long–lived aggregated storms which deliver intense convective downpours and extensive stratiform rainfall, shaping both hydroclimatic extremes and, via diabatic heating, tropical energy budgets (R. Schumacher & Rasmussen, 2020).

MCSs are poorly represented in coarse–grid operational global circulation models (GCMs), which parameterize convection (Slingo et al., 2022). Typical parameterization schemes cannot capture the fundamental interaction of multi–scale processes within MCSs (Moncrieff et al., 2017; Prein et al., 2015). This deficiency yields poor fidelity when compared to convection–permitting (CP) models that explicitly represent convective motion: CP models

more realistically simulate MCS lifecycles, propagation, and rainfall rates (Crook et al., 2019; Prein et al., 2017; Senior et al., 2021), increasing projections of future storm rainfall extremes (Kendon et al., 2019; Kooperman et al., 2014). Improved simulation of MCSs also has remote effects. Midlatitude summer forecast skill is tied to remote storm hotspots (Pante & Knippertz, 2019; Rodwell et al., 2013), while explicitly representing convection modifies large–scale circulations (Hart et al., 2018; Morris et al., 2024).

The manifold interactions which integrate deep–convective processes into all scales of the climate system have inspired proposals for programmes of global CP climate modeling (Slingo et al., 2022; Stevens et al., 2023). Such proposals are supported by model progress: the DYAMOND intercomparison showcased a panoply of 40 days global kilometer–scale models (Stevens et al., 2019), while multi–year coupled simulations are already yielding new insights (Lee & Hohenegger, 2024; Segura et al., 2022). However, expanding global CP modeling necessitates enormous financial and institutional resources. Rigorous process–based evaluation is essential to justify such expenditure. For example, evaluation of MCS characteristics across DYAMOND models by Feng et al. (2023) found significant variation, which must be understood. CP models remain reliant on parameterizations of sub–grid processes such as microphysics and turbulent mixing (Kendon et al., 2021; Prein et al., 2021; Tomassini et al., 2023). Treatments of these processes vary between models and significantly affect overall biases (Feng et al., 2018).

An under–explored bias is representation of the observed response of MCS rainfall extremes to thermodynamic (atmospheric moisture, CAPE) and dynamical (low–level wind shear) environments (Feng et al., 2016; Fitzpatrick et al., 2020). The role of shear extends beyond facilitating convective aggregation to influencing mature MCS characteristics (Chen et al., 2023; Rotunno et al., 1988; Taylor et al., 2017). Shear modulates storm inflow (Alfaro, 2017; Bickle et al., 2021), with updraft buoyancy enhanced in strong shear environments due to increases in core updraft size and corresponding decreases in entrainment–dilution (Mulholland et al., 2021). This dynamical control explains observed African MCS anvil heights (Baidu et al., 2022) and increases in idealized MCS rainfall extremes (Abramian et al., 2023).

Given their critical role in hydrological extremes, the physics of MCS responses to environmental drivers must be both understood and faithfully represented in models. Concerningly, CP models can fail to capture MCS rainfall–shear responses (Senior et al., 2021). We therefore investigate MCS environmental controls in Met Office Unified Model (MetUM) CP simulations, focusing on shear. In Section 3.1 we quantify the influence of such controls in models and observations, then showing that models' MCS rainfall–shear responses depend on shear–induced entrainment variability (Section 3.2). We demonstrate that shear exerts controls on MCS mean rainfall and anvil heights. Moreover, we show shear explains zonal distributions of MCS mean rainfall biases (Section 3.3), shifting atmospheric heating patterns and thus influencing the forcing of tropical circulation.

2. Model and Observational Data

Our focus is MCSs over West Africa (4°–25°N, −18°–25°E, land only), a global hotspot for MCS activity with strong meridional gradients in zonal wind shear and atmospheric moisture. We utilize four regional implementations of the non–hydrostatic, semi–Lagrangian MetUM (Brown et al., 2012), each covering at least one 40 days DYAMOND summer period (01/08–09/09). CP models are of primary interest; understanding MCSs in parameterized models is complicated by systematic biases such as widespread low rainfall and an earlier diurnal peak in convection (e.g., Crook et al. (2019)), however for completeness we follow a common methodology including parameterized results. Model domains are shown in Figure S1 in Supporting Information S1, with all data sets limited to the DYAMOND date window.

Trop5–exp and Trop5–param are both a pan–longitudinal Cyclic Tropical Channel (CTC) covering one DYAMOND summer (2016). Both models use 90 vertical levels up to 40 km and a horizontal N2560 grid, equating to ∼5 km latitudinal and ∼8 km longitudinal resolution at the equator. Latitudinal boundary conditions (BCs) are driven hourly by a ∼10 km (N1280) global simulation initialized from a MetUM operational analysis, whereas longitudinally moisture, energy and momentum across scales can propagate over the dateline. We further include a 2.2 km resolution Limited Area Model (LAM) covering northern Africa over the same period (01/08/2016–09/09/2016), LAM2.2, which also derives BCs from the N1280 simulation (Jones et al., 2023). LAM2.2 has the same vertical levels as the CTCs. For all three models hourly surface diagnostics and 3–hourly profile fields are available.

Both Trop5–exp and LAM2.2 represent convection explicitly (RAL3.2 science configuration, Bush et al. (2023)), whereas in Trop5–param a CAPE–closure mass flux parametrization is used (GAL9.1 science configuration, Walters et al. (2019)). This is the primary difference between the configurations. RAL3.2 also uses CASIM double moment cloud microphysics and bimodal large–scale cloud parametrization schemes (Field et al., 2023; Van Weverberg et al., 2021), whereas in GAL9.1 these are single moment Wilson–Ballard microphysics and PC2 prognostic cloud, respectively (Wilson & Ballard, 1999; Wilson et al., 2008). The chosen science configurations represent the most advanced CP and parameterized modeling setups presently available in the MetUM. All three models are forced by daily updating SSTs and an explicitly represented land surface (Best et al., 2011).

To assess the impact of model physics we feature a previous generation MetUM climate simulation, CP4–Af, a 4.5 km grid pan–African model spanning 1997 to 2007, with 80 vertical levels up to 40 km (Stratton et al., 2018). The simulation was driven by three–hourly lateral BCs from a 30–years, GA7.1 N512 resolution global model and by observed daily sea surface temperatures. CP4–Af utilizes explicit deep convection, Wilson–Ballard single moment microphysics, the Smith prognostic cloud scheme (Smith, 1990), and a coupled land–surface with uniform sandy soil. Although this configuration substantially improved representation of convective organisation versus parameterized counterparts (Crook et al., 2019; Senior et al., 2021), CP4–Af failed to capture realistic MCS maxmimum rainfall–shear responses (Fitzpatrick et al., 2020; Klein et al., 2021).

For all models we sample MCSs between 16 and 21UTC, the hours of peak convection over West Africa. Following Klein et al. (2021), MCSs are identified hourly as snapshots of contiguous cloud brightness temperature (BT) $\leq -50°C$ that have an area greater than 5000 km^2 and maximum precipitation rate ≥ 1 mm hr^{-1}. Here model BT fields are obtained from TOA outgoing longwave radiation using the empirical conversion of Yang and Slingo (2001). Environmental conditions preceding an MCS are taken as 12UTC mean fields across a 0.7° box centered on the location of the storm's minimum BT, that is, the most intense convective core.

Where possible, model results are compared against MCSs identified by applying the same BT threshold and area criteria to hourly, 0.1° Meteosat Second Generation 10.8μm–band observed BTs spanning 2000–2019. Observed MCS precipitation features are sampled using microwave–only precipitation estimates of V06 B Integrated Multi–satellitE Retrievals for Global Precipitation Measurement (GPM–IMERG–HQ) data (Huffman et al., 2019) at ~15 km spatial and 30 min temporal resolution. Environmental fields are then calculated in the same manner as in models from 12UTC ERA5 profiles (Hersbach et al., 2020). We denote the combination of reanalysis and satellite products OBS.

MCS environmental controls are identified by binning MCS variables by environmental fields, with histograms taken between 5th and 95th percentile axis values to remove extreme conditions. A minimum threshold of 5 MCSs is applied to all histogram bins. Environmental scalings are quantified using error–weighted linear regression applied to 1D histograms. Assessments of statistical significance use 2–sided t–tests.

3. Environmental Controls

3.1. MCS Extremes

Figure 1 shows relationships over West Africa of maximum MCS rainfall to environmental total column water (TCW) and the difference between 650 hPa and 850 hPa zonal winds ($u650 - u850$, easterly positive; levels of African Easterly Jet and south-westerly monsoon respectively), henceforth labeled (low–level) shear. MCS spatial distributions and mean 12UTC TCW and shear are plotted in Figures S2 and S3 in Supporting Information S1. These fields represent storms' thermodynamic and dynamical environments respectively, and manifest independent MCS influences: in OBS, the shear–TCW correlation is −0.08 ($p < 0.01$).

The OBS panel in Figure 1a shows that West African MCS rainfall extremes are maximized in very moist, strong shear environments — there are both thermodynamic, and dynamical, controls on MCS rainfall (distributions in Figure S4 in Supporting Information S1). Figures 1b and 1c isolate the environmental influences by calculating reduced 1D histograms. The scalings δ of maximum rainfall with TCW and shear respectively (green lines) are of similar magnitude, indicating equal influences on storm extremes. This is not the case in CP4–Af, where despite the explicit representation of convective dynamics, only the thermodynamic control is resolved: the highest rainfall maxima occur across all high–TCW shear regimes. The model scaling (gold) with TCW is realistic, but for shear the scaling ratio $\delta/\delta_{obs} \sim 0.20$.
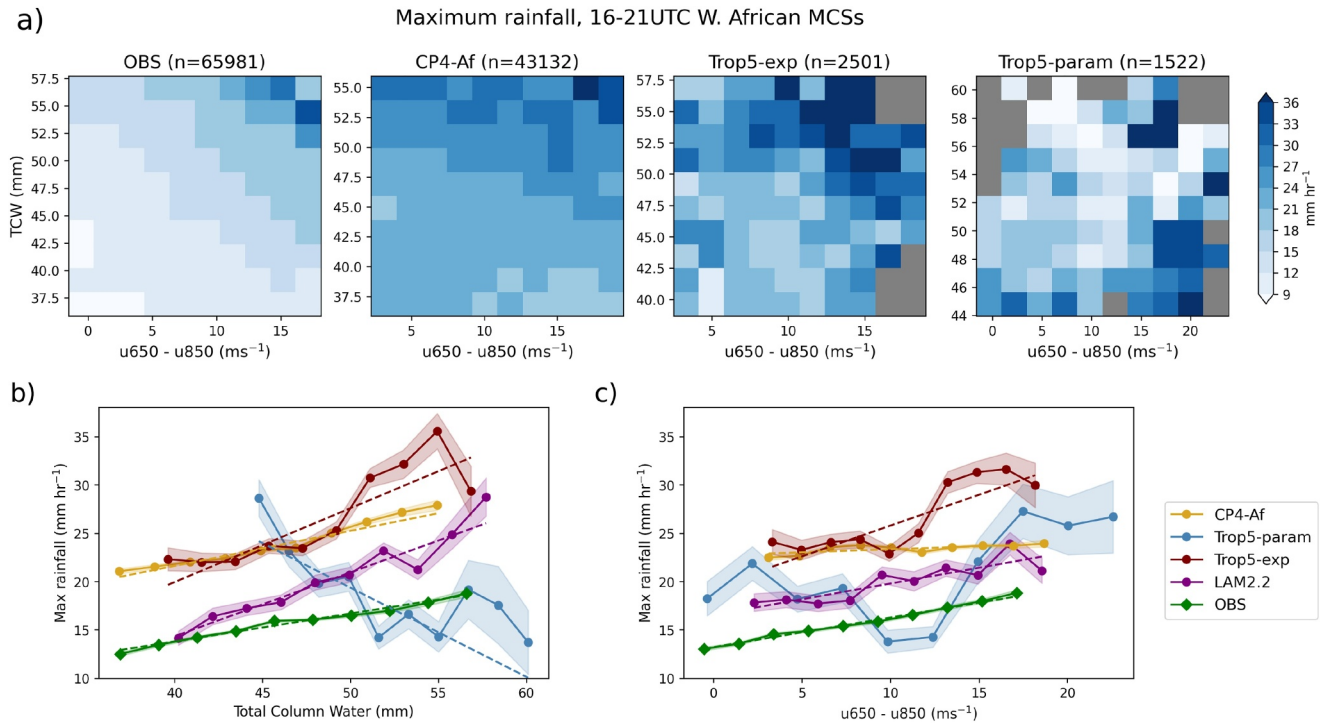
Figure 1. Maximum MCS rainfall, binned by (a) TCW and shear, (b) TCW only, and (c) shear only. Values n indicate number of MCS s, $n_{lam} = 2910$. Shading in line plots denotes standard error on bin mean. Dashed lines indicate trend for error–weighted regression where gradient and correlation are significant at 95% level.

In current generation MetUM models we find scalings of maximum MCS rainfall with both shear and TCW. The Trop5–exp panel in Figure 1a shows the highest MCS rainfall maxima are generated by strong shear and high TCW environments (LAM2.2 similar, Figure S5 in Supporting Information S1). The environmental responses are generally stronger than observed, especially for TCW, but the overall balance of thermodynamic and dynamical controls is more realistic than CP4–Af: in LAM2.2 (purple lines) the TCW scaling is twice as strong as in OBS, but the shear scaling is statistically indistinguishable ($p = 0.76$). For Trop5–exp (maroon) the shear scaling is also twice as strong ($p = 0.01$).

The linear scalings of the CP models and OBS are not found in Trop5–param. While MCS maximum rainfall does show an overall increase with shear, for TCW the relationship is reversed (significant correlation, $p = 0.01$). Figure S6 in Supporting Information S1 shows that the scaling is due to very high explicit rainfall values, colocated with the highest explicit updraft velocities, overwhelming the parameterized rainfall contribution at low TCW. This highlights the challenge of representing convection at these scales (Tomassini et al., 2023).

The improvement in MCS shear response between the CP model generations cannot be explained by grid spacing, suggesting that changes to physics schemes have led to fundamental differences in the treatments of MCS organisation and updraft physics. MCS anvil areas in CP4–Af are 40% smaller than OBS on average and show limited environmental variability (Figure S7 in Supporting Information S1), in contrast to OBS and current generation models. Furthermore for two measures of convective core strength, minimum MCS cloud BT (Figure S8 in Supporting Information S1) and maximum 500 hPa vertical velocity $w500_{max}$ (Figure S9 in Supporting Information S1), CP4–Af shows much weaker environmental dependence than Trop5–exp and LAM2.2. In the case of minimum BT, which can be reliably identified for observed storms, those models' shear scalings are statistically indistinguishable from OBS ($p > 0.5$), whereas the CP4–Af scaling is 75% weaker. These results hint at a possible role of updraft entrainment.

3.2. Updraft Entrainment

The role of entrainment is demonstrated by Figure 2, which shows that models with realistic dynamical controls on maximum MCS rainfall (Trop5–exp and LAM2.2) exhibit weaker updraft entrainment–dilution in strong shear
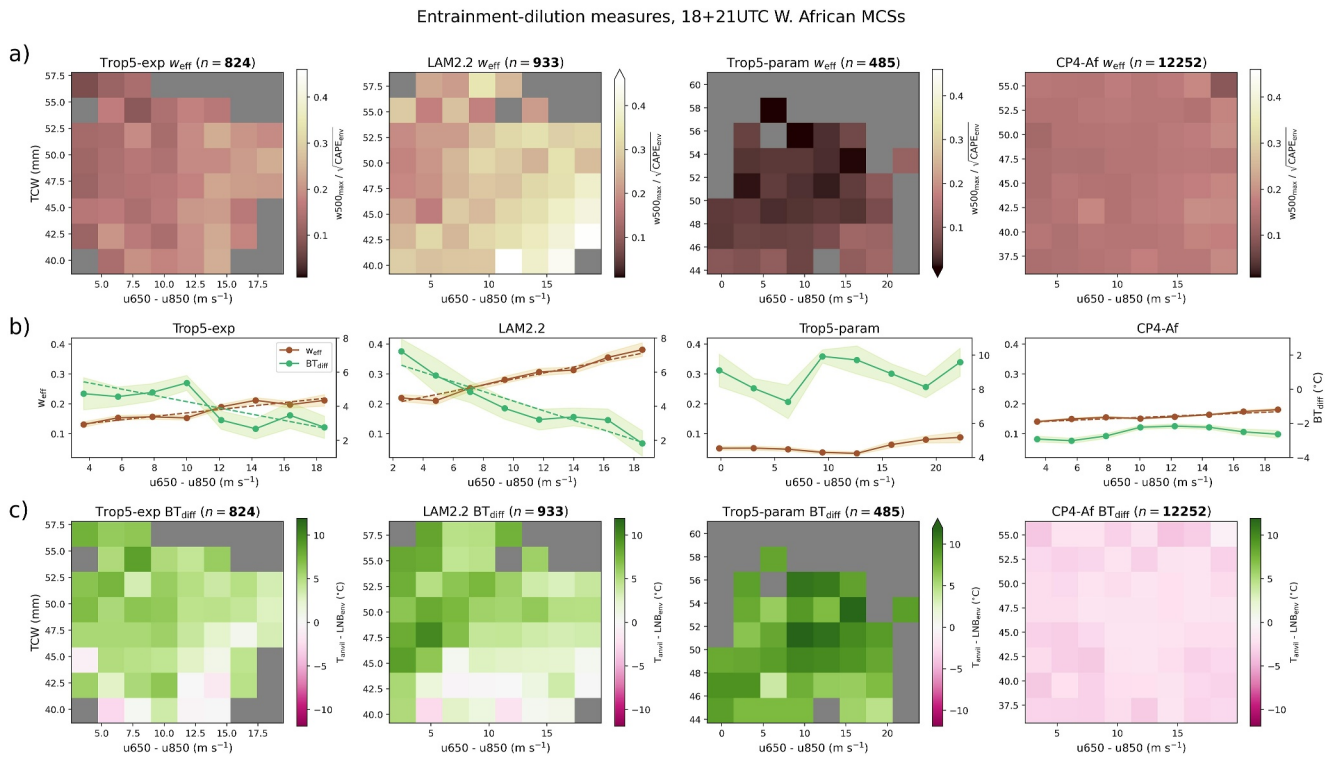
Figure 2. Scaling of model MCS entrainment proxies w_{eff} (a; brown in (b) and BT_{diff} (c; green in (b) binned by TCW and shear. Common variable histograms share absolute colourbars, whereas line plots share relative axis ranges. Number of MCSs n for 18 and 21UTC only due to 3 hourly profile fields. Line plots as in Figure 1.

environments. We use two complementary proxies for entrainment: the efficiency w_{eff} of conversion of environmental CAPE ($CAPE_{env}$) to MCS $w500_{max}$, and difference BT_{diff} between mean anvil BT (T_{anv}) and environmental Level of Neutral Buoyancy (LNB_{env}), with soundings taken from mean environmental profiles. High w_{eff} and low BT_{diff} imply reduced entrainment–dilution since entrainment reduces the potential of a near–surface parcel to reach its theoretical maximum buoyancy, reducing vertical velocities and lowering anvils. For Trop5–exp and LAM2.2 (LH columns) high w_{eff} and low BT_{diff} values are found in strong shear environments, and to a lesser–extent, low TCW (consistent with Becker and Hohenegger (2021)). In contrast, MCSs in CP4–Af and Trop5–param show minimal variability of entrainment with environmental shear (or TCW). In the parameterized model entrainment into explicit updrafts is high across all but the driest environments, whereas CP4–Af likely shows underestimated dilution across all environments, in line with other previous generation CP models (Prein et al., 2021). There is a significant correlation ($p < 0.05$) between shear–binned MCS w_{eff} and maximum rainfall in all models: the lack of a dynamical influence on entrainment explains the absence of a rainfall–shear response in CP4–Af.

Dynamical entrainment variability is of greater consequence for rainfall scalings than thermodynamic: in Trop5–exp and LAM2.2 the (weak) control of TCW on entrainment is the opposite sign to that for MCS maximum rainfall, while CP4–Af shows a realistic maximum rainfall–TCW scaling despite no entrainment variation. Our results for Trop5–exp and LAM2.2 align with previous observational findings for African MCSs (Baidu et al., 2022). We also find that MCSs' dynamical environments exert a strong influence on observed anvil heights (Figure S10 in Supporting Information S1), as implied by results for BT_{diff}. This trend is realistically captured by both Trop5–exp and LAM2.2 (lowest scaling ratio LAM2.2, $\delta/\delta_{obs} \sim 0.85$), but not CP4–Af ($\delta/\delta_{obs} \sim 0.32$).

Large–eddy simulations indicate that reduced entrainment–dilution in strong shear environments is a result of a positive influence of shear on MCS convective core size (Mulholland et al., 2021). We examine the scalings of explicitly modeled core areas in Figure 3. To define convective cores we identify contiguous subregions of MCS anvil footprints where w500 is greater than the 99th percentile of its in–storm values. The percentile threshold accounts for models' different vertical velocity distributions. Where multiple cores are identified we select that with the maximum value of w500; in all models core area correlates strongly with $w500_{max}$ (not shown).
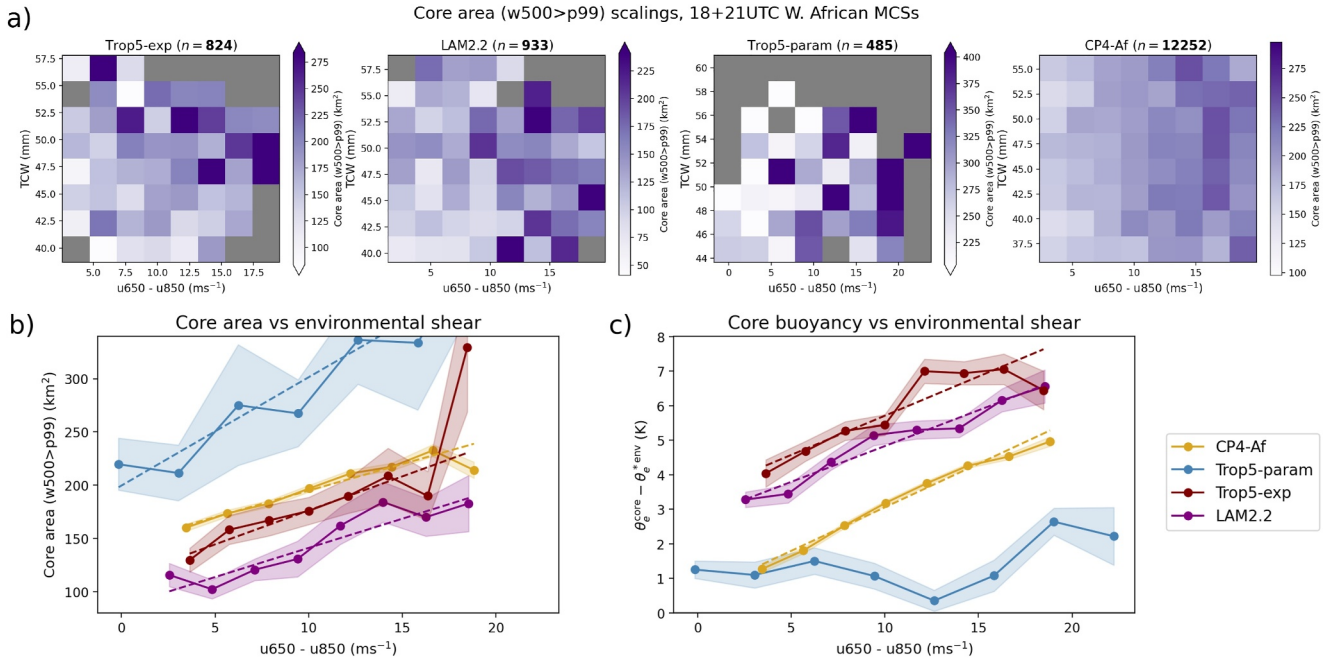
Figure 3. Area of strongest MCS explicit updraft cores, binned by (a) TCW and shear, and (b) shear only. Number of MCSs *n* for 18 and 21UTC only; histograms share common scale range. (c) Core buoyancy binned by shear. Line plots as in Figure 1.

MCSs in all models have larger cores in stronger shear environments (Figure 3). The shear scalings are strongest for Trop5–exp and LAM2.2, as expected from Figure 2, but here CP4–Af and Trop5–param also show variable core areas. Indeed, the shear–only scaling in Figure 3b shows no significant difference between the CP models ($p > 0.4$), but is twice as strong for Trop5–param. In all models except Trop5–exp there is no significant correlation between updraft core size and environmental TCW (Figure S11a in Supporting Information S1). The significant relationship with shear alone supports the proposal of Mulholland et al. (2021) that dynamical influences on MCS core size lead to the variation of updraft entrainment with shear. It is this physics which is missing in CP4–Af and Trop5–param.

A physical effect of the increase of core area with shear, well captured by all three CP models, is an increase in core buoyancy. This is calculated as the 500 hPa difference between θ_e^{core}, the mean core equivalent potential temperature at that level, and $\theta_e^{*\mathrm{env}}$, the environmental value for a saturated profile. Figure 3c shows that more buoyant updrafts are found in stronger shear environments for all models, but that the scaling for Trop5–param is very weak, at approximately 10% of the CP models. Core buoyancy decreases with environmental TCW (Figure S11b in Supporting Information S1); the scaling is stronger than for shear in Trop5–param, but weak in all CP models (at most 50% vs. shear, LAM2.2). Given MCS rainfall shows the opposite scaling with TCW (Figure 1), buoyancy can mediate the dynamical (shear) dependence only.

3.3. Upscale Forcings

We now consider whether environmental controls influence MCS mean rainfall and carry upscale implications. Figures 4a and 4b show that for OBS, MCS hourly mean rainfall (total MCS rainfall/anvil area) has a positive non–linear scaling with environmental TCW, and weaker (but significant, $p = 0.00$) linear influence from shear. All CP models capture the general non–linear TCW scaling, particularly the strong increase of mean rainfall at high TCW. Mean rainfall rates are too low in LAM2.2, with MCSs on average 20% larger than OBS (Figure S7 in Supporting Information S1). Trop5–param shows a negative relationship between TCW and MCS mean rainfall, for the same reasons as maximum rainfall (Figure S6 in Supporting Information S1).

In contrast, for shear there are again systematic differences between CP4–Af and current generation CP models. MCS mean rainfall decreases with shear in CP4–Af, opposite to the observed relationship. Meanwhile Trop5–exp and LAM2.2 both capture a significant positive influence ($r > 0.6$), but in Trop5–param there is no relationship
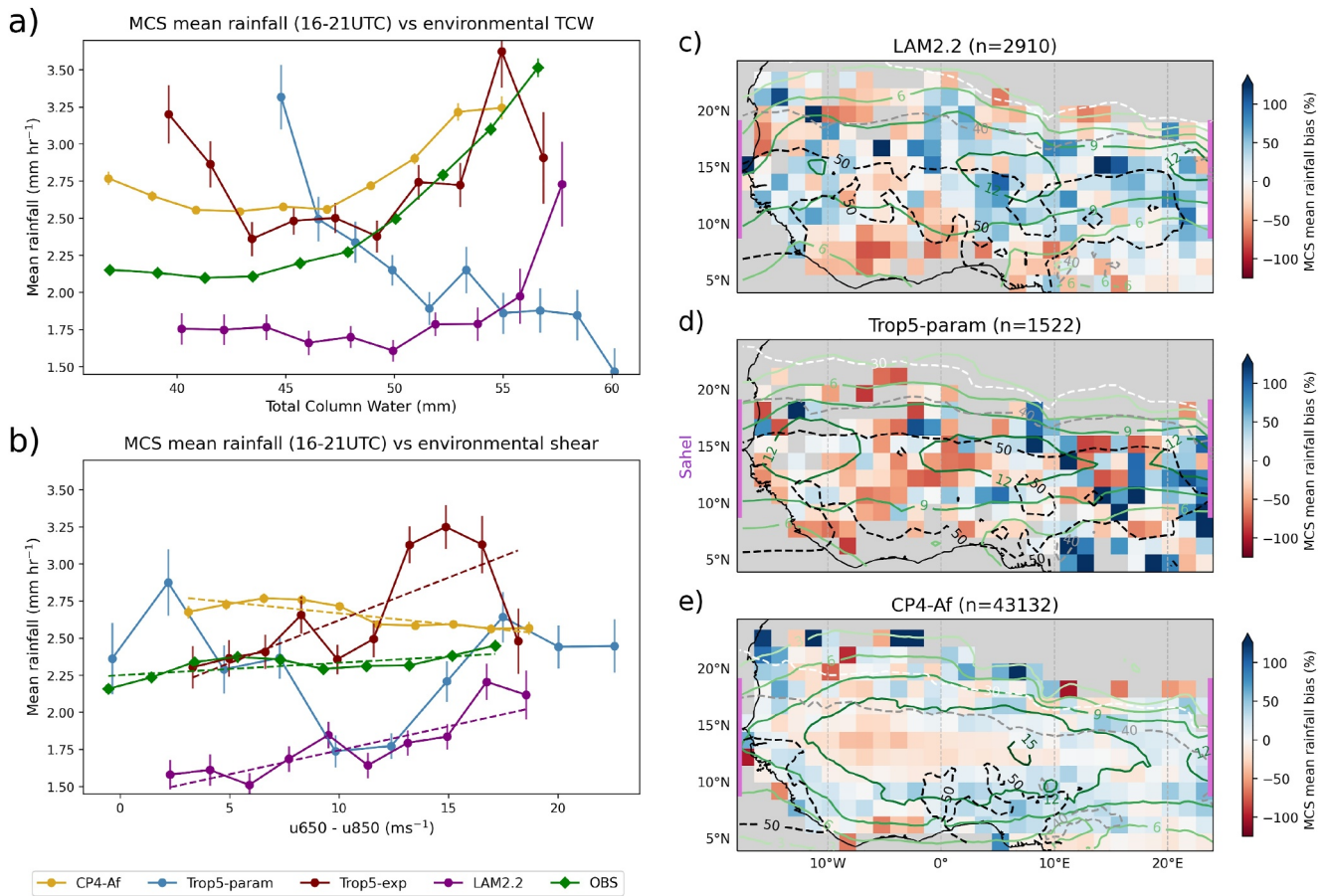
Figure 4. MCS mean rainfall binned by (a) TCW and (b) shear. Panels (c)–(e) show 1.5° mean MCS rainfall spatial biases against OBS for LAM2.2, Trop5–param and CP4–Af anomalies, respectively. Error bars show standard error on bin, with dashed lines in (b) as in Figure 1. Spatial biases expressed as percentage of OBS anomaly; number of MCSs n covers all hours, $n_{obs} = 65,981$. In spatial plots, green (gray dashed) contours show 12UTC model mean shear (TCW) fields, units ms^{-1} (mm). Pink bars indicate Sahel latitudes.

($r = -0.05$). The positive shear scalings are too strong, with for example, $\delta/\delta_{obs} \sim 3.87$ in LAM2.2, and the Trop5–exp trend showing notable uncertainty. Nevertheless, these scalings reflect those for updraft entrainment. A significant correlation between the w_{eff} and mean rainfall scalings in all CP models indicates that the influence of shear–induced entrainment variability extends to total rainfall.

To explore upscale impacts stemming from environmental drivers we consider spatial biases of MCS mean rainfall anomalies (isolating scalings) versus OBS. Although TCW controls are stronger, differences in models' shear responses explain the spatial bias patterns: LAM2.2 (Figure 4c) shows a wet bias across the north of the Sahel (9°–19°N) region where low–level shear peaks, and dry biases in weaker shear regions, independent of TCW and in line with the model's strong shear scaling. The correlation between zonal MCS mean rainfall bias and shear is $r = 0.67$ (0.01), with no significant correlation against zonal mean TCW ($p = 0.24$). Trop5–param biases are noisy (Figure 4d), with no significant (zonal) correlation against TCW or shear, reflecting the model's absent shear scaling. However, CP4–Af (Figure 4e) shows the opposite distribution of MCS biases: the negative relationship between MCS mean rainfall and shear corresponds to dry biases in the strong–shear Sahel, with zonal correlation $r = -0.57$ (0.04)), and wet biases across all TCW regimes at low shear. Strikingly, the biases in Figure 4e reflect CP4–Af's seasonal JJA rainfall bias (Fig. 5, Stratton et al. (2018)), indicating the potential upscale propagation of errors stemming from the incorrect MCS shear response.

4. Discussion and Conclusions

The dynamics of MCSs are strongly influenced by environmental conditions. We have studied the fidelity of these influences in four MetUM simulations, demonstrating the importance of model physics for capturing storms' response to low–level shear.

Our results show that representative current generation CP models (Trop5–exp and LAM2.2) have increased MCS maximum and mean rainfall with stronger low–level shear, in agreement with observations. Higher shear gives larger convective cores with higher buoyancies and, crucially, lower entrainment–dilution, consistent with the numerical experiments of Mulholland et al. (2021). Rainfall increases with environmental TCW via thermodynamic controls independent of core dynamics. Results for parameterized MCSs (Trop5–param) show larger explicit cores at stronger shear, but no translation to buoyancy, entrainment and consequently, maximum and mean rainfall rates. The influence of shear on parameterized MCSs is thus underestimated. Trop5–param also shows unrealistic negative correlations between TCW and MCS rainfall, caused by strong explicit contributions overwhelming the parameterization scheme at low TCW.

A previous generation CP climate simulation (CP4–Af) does capture the thermodynamic response of MCS rainfall, and shows larger cores with higher buoyancies at stronger shear. However, CP4–Af shows no environmental variability of updraft entrainment. This causes unrealistically limited shear responses for key characteristics such as MCS maximum rainfall and brightness temperatures, which are overestimated at low shear, and an erroneous decrease in mean rainfall with shear. Becker and Hohenegger (2021) emphasize the importance of mesoscale organisation in increasing West African entrainment rates; this is arguably underestimated in CP4–Af (e.g., small anvil areas, Figure S7 in Supporting Information S1), possibly yielding the uniform low entrainment found in Figure 2. The contrasting behavior between different generation CP models highlights the paramount importance of both model physics development and process–based model evaluation.

The influence of MCSs' thermodynamic and dynamical environments extends beyond updrafts to whole–storm characteristics. Anvil heights play an important role in tropical radiation budgets, while latent heat release from MCS stratiform rainfall regions provides a strong upscale forcing on tropical circulations from top–heavy heating profiles (C. Schumacher et al., 2004). An observed decrease in anvil temperature of -0.24°C per unit shear increase (Figure S10 in Supporting Information S1) equates to a net change in TOA cooling of 1.81×10^{-10} Wm^{-2}, assuming a blackbody. This is dwarfed by latent heating, for which the observed linear scaling (Figure 4b) equates to 5.25 Wm^{-2} per unit shear. Neither scaling is accurately represented by CP–Af or Trop5–param.

We have presented evidence indicating that the dynamical control of shear explains the regional distribution of MCS mean rainfall biases. Mean rainfall, and therefore diabatic heating, anomalies for LAM2.2 MCSs in the central Sahel are over 100% stronger than for storms in CP4–Af, with the inverse true near the coast, together suggesting a more realistic monsoon pattern when shear control is captured (Stratton et al., 2018). Diabatic heating from West African MCSs affects potential vorticity distributions (Johnson & Ciesielski, 2020) and the development of African Easterly Waves (Tomassini et al., 2017), which further play a role in the development of Atlantic tropical cyclones (Núñez Ocasio et al., 2020). Zonal changes in MCS heating profiles, modulated by shear, will influence model representation of all these processes. Detailed analysis of upscale impacts in current generation MetUM configurations should be pursued in longer simulations than those presented here.

Our results have consequences for current and future climate modeling endeavors. Multi–year CP modeling is feasible for the coupled climate system (Rackow et al., 2024), and may be essential for providing accurate hydroclimatic projections (Slingo et al., 2022). To justify and support their adoption, global CP models must demonstrate upscale gross benefits directly emanating from the improved treatment of fundamental convective processes. Here we have demonstrated the importance of updraft entrainment for resolving realistic MCS rainfall–shear responses, and indicated that this dynamical control has upscale impacts. Such process–based evaluation of convective interactions across scales thus provides insight into large–scale model attributes, and is an imperative component of next generation GCM development.

Data Availability Statement

Code and data underpinning this research are available publicly at Maybee et al. (2024).

References

Abramian, S., Muller, C., & Risi, C. (2023). Extreme precipitation in tropical squall lines. *Journal of Advances in Modeling Earth Systems*, *15*(10), e2022MS003477. https://doi.org/10.1029/2022MS003477

Alfaro, D. A. (2017). Low–tropospheric shear in the structure of squall lines: Impacts on latent heating under layer–lifting ascent. *Journal of the Atmospheric Sciences*, *74*(1), 229–248. https://doi.org/10.1175/JAS-D-16-0168.1

Baidu, M., Schwendike, J., Marsham, J. H., & Bain, C. (2022). Effects of vertical wind shear on intensities of mesoscale convective systems over West and Central Africa. *Atmospheric Science Letters*, *23*(8), e1094. https://doi.org/10.1002/asl.1094

Becker, T., & Hohenegger, C. (2021). Entrainment and its dependency on environmental conditions and convective organization in convection–permitting simulations. *Monthly Weather Review*, *149*(2), 537–550. https://doi.org/10.1175/MWR-D-20-0229.1

Best, M. J., Pryor, M., Clark, D. B., Rooney, G. G., Essery, R., Ménard, C. B., et al. (2011). The Joint UK Land Environment Simulator (JULES), model description–Part 1: Energy and Water Fluxes. *Geoscientific Model Development*, *4*(3), 677–699. https://doi.org/10.5194/gmd-4-677-2011

Bickle, M. E., Marsham, J. H., Ross, A. N., Rowell, D. P., Parker, D. J., & Taylor, C. M. (2021). Understanding mechanisms for trends in Sahelian squall lines: Roles of thermodynamics and shear. *Quarterly Journal of the Royal Meteorological Society*, *147*(735), 983–1006. https://doi.org/10.1002/qj.3955

Bony, S., Semie, A., Kramer, R. J., Soden, B., Tompkins, A. M., & Emanuel, K. A. (2020). Observed modulation of the tropical radiation budget by deep convective organization and lower-tropospheric stability. *AGU Advances*, *1*(3), e2019AV000155. https://doi.org/10.1029/2019AV000155

Bony, S., Stevens, B., Frierson, D. M., Jakob, C., Kageyama, M., Pincus, R., et al., (2015). Clouds, circulation and climate sensitivity. *Nature Geoscience*, *8*(4), 261–268. https://doi.org/10.1038/ngeo2398

Brown, A., Milton, S., Cullen, M., Golding, B., Mitchell, J., & Shelly, A. (2012). Unified modeling and prediction of weather and climate: A 25–year journey. *Bulletin of the American Meteorological Society*, *93*(12), 1865–1877. https://doi.org/10.1175/BAMS-D-12-00018.1

Bush, M., Boutle, I., Edwards, J., Finnenkoetter, A., Franklin, C., Hanley, K., et al. (2023). The second Met Office Unified Model–JULES Regional Atmosphere and Land configuration, RAL2. *Geoscientific Model Development*, *16*(6), 1713–1734. https://doi.org/10.5194/gmd-16-1713-2023

Chen, X., Leung, L. R., Feng, Z., & Song, F. (2022). Crucial Role of Mesoscale Convective Systems in the Vertical Mass, Water, and Energy Transports of the South Asian Summer Monsoon. *Journal of Climate*, *35*(1), 91–108. https://doi.org/10.1175/JCLI-D-21-0124.1

Chen, X., Leung, L. R., Feng, Z., & Yang, Q. (2023). Environmental controls on MCS lifetime rainfall over tropical oceans. *Geophysical Research Letters*, *50*(15), e2023GL103267. https://doi.org/10.1029/2023GL103267

Crook, J., Klein, C., Folwell, S., Taylor, C. M., Parker, D. J., Stratton, R., & Stein, T. (2019). Assessment of the representation of West African storm lifecycles in convection-permitting simulations. *Earth and Space Science*, *6*(5), 818–835. https://doi.org/10.1029/2018EA000491

Feng, Z., Leung, L. R., Hagos, S., Houze, R. A., Burleyson, C. D., & Balaguru, K. (2016). More frequent intense and long-lived storms dominate the springtime trend in central US rainfall. *Nature Communications*, *7*(1), 13429. https://doi.org/10.1038/ncomms13429

Feng, Z., Leung, L. R., Hardin, J., Terai, C. R., Song, F., & Caldwell, P. (2023). Mesoscale Convective Systems in DYAMOND Global Convection–Permitting Simulations. *Geophysical Research Letters*, *50*(4), e2022GL102603. https://doi.org/10.1029/2022GL102603

Feng, Z., Leung, L. R., Houze Jr, R. A., Hagos, S., Hardin, J., Yang, Q., et al. (2018). Structure and Evolution of Mesoscale Convective Systems: Sensitivity to Cloud Microphysics in Convection–Permitting Simulations over the United States. *Journal of Advances in Modeling Earth Systems*, *10*(7), 1470–1494. https://doi.org/10.1029/2018MS001305

Field, P. R., Hill, A., Shipway, B., Furtado, K., Wilkinson, J., Miltenberger, A., et al. (2023). Implementation of a double moment cloud microphysics scheme in the UK Met Office regional numerical weather prediction model. *Quarterly Journal of the Royal Meteorological Society*, *149*(752), 703–739. https://doi.org/10.1002/qj.4414

Fitzpatrick, R. G., Parker, D. J., Marsham, J. H., Rowell, D. P., Guichard, F. M., Taylor, C. M., et al. (2020). What Drives the Intensification of Mesoscale Convective Systems over the West African Sahel under Climate Change? *Journal of Climate*, *33*(8), 3151–3172. https://doi.org/10.1175/JCLI-D-19-0380.1

Hart, N. C., Washington, R., & Stratton, R. A. (2018). Stronger local overturning in convective–permitting regional climate model improves simulation of the subtropical annual cycle. *Geophysical Research Letters*, *45*(20), 11–334. https://doi.org/10.1029/2018GL079563

Hersbach, H., Bell, B., Berrisford, P., Hirahara, S., Horányi, A., Muñoz-Sabater, J., et al., (2020). The ERA5 global reanalysis. *Quarterly Journal of the Royal Meteorological Society*, *146*(730), 1999–2049. https://doi.org/10.1002/qj.3803

Huffman, G. J., Bolvin, D. T., Nelkin, E. J., & Tan, J. (2019). GPM IMERG final precipitation L3 half hourly 0.1 degree $\times$ 0.1 degree V06. *Earth Sciences Data and Information Services Center (GES DISC)*, *01*. Retrieved from https://disc.gsfc.nasa.gov/datasets/GPM3IMERGHH06/summary

Johnson, R. H., & Ciesielski, P. E. (2020). Potential vorticity generation by West African squall lines. *Monthly Weather Review*, *148*(4), 1691–1715. https://doi.org/10.1175/MWR-D-19-0342.1

Jones, R. W., Sanchez, C., Lewis, H., Warner, J., Webster, S., & Macholl, J. (2023). Impact of domain size on tropical precipitation within explicit convection simulations. *Geophysical Research Letters*, *50*(17), e2023GL104672. https://doi.org/10.1029/2023GL104672

Kendon, E. J., Prein, A. F., Senior, C. A., & Stirling, A. (2021). Challenges and outlook for convection–permitting climate modelling. *Philosophical Transactions of the Royal Society A*, *379*(2195), 20190547. https://doi.org/10.1098/rsta.2019.0547

Kendon, E. J., Stratton, R. A., Tucker, S., Marsham, J. H., Berthou, S., Rowell, D. P., & Senior, C. A. (2019). Enhanced future changes in wet and dry extremes over Africa at convection-permitting scale. *Nature Communications*, *10*(1), 1794. https://doi.org/10.1038/s41467-019-09776-9

Klein, C., Jackson, L. S., Parker, D. J., Marsham, J. H., Taylor, C. M., Rowell, D. P., et al. (2021). Combining CMIP data with a regional convection-permitting model and observations to project extreme rainfall under climate change. *Environmental Research Letters*, *16*(10), 104023. https://doi.org/10.1088/1748-9326/ac26f1

Kooperman, G. J., Pritchard, M. S., & Somerville, R. C. (2014). The response of us summer rainfall to quadrupled CO_2 climate change in conventional and superparameterized versions of the NCAR community atmosphere model. *Journal of Advances in Modeling Earth Systems*, *6*(3), 859–882. https://doi.org/10.1002/2014MS000306

Lee, J., & Hohenegger, C. (2024). Weaker land–atmosphere coupling in global storm-resolving simulation. *Proceedings of the National Academy of Sciences*, *121*(12), e2314265121. https://doi.org/10.1073/pnas.2314265121

Maybee, B., Klein, C., & Barton, E. (2024). BMaybee/MCS_shear_evaluation: MCS_shear_evaluation_v1 (zenodo). [Software]. *Zenodo*. https://doi.org/10.5281/zenodo.11110361

Moncrieff, M. W., Liu, C., & Bogenschutz, P. (2017). Simulation, modeling, and dynamically based parameterization of organized tropical convection for global climate models. *Journal of the Atmospheric Sciences*, *74*(5), 1363–1380. https://doi.org/10.1175/JAS-D-16-0166.1

Morris, F., Schwendike, J., Parker, D. J., & Bain, C. (2024). How is Synoptic-Scale Circulation Influenced by the Dynamics of Mesoscale Convection in Convection-Permitting Simulations over West Africa? *Journal of the Atmospheric Sciences*, *81*(4), 765–782. https://doi.org/10.1175/JAS-D-22-0032.1

Mulholland, J. P., Peters, J. M., & Morrison, H. (2021). How does vertical wind shear influence entrainment in squall lines? *Journal of the Atmospheric Sciences*, *78*(6), 1931–1946. https://doi.org/10.1175/JAS-D-20-0299.1

Núñez Ocasio, K. M., Evans, J. L., & Young, G. S. (2020). A wave-relative framework analysis of AEW–MCS interactions leading to tropical cyclogenesis. *Monthly Weather Review*, *148*(11), 4657–4671. https://doi.org/10.1175/MWR-D-20-0152.1

Pante, G., & Knippertz, P. (2019). Resolving Sahelian thunderstorms improves mid-latitude weather forecasts. *Nature Communications*, *10*(1), 3487. https://doi.org/10.1038/s41467-019-11081-4

Prein, A. F., Langhans, W., Fosser, G., Ferrone, A., Ban, N., Goergen, K., et al. (2015). A review on regional convection-permitting climate modeling: Demonstrations, prospects, and challenges. *Reviews of Geophysics*, *53*(2), 323–361. https://doi.org/10.1002/2014RG000475

Prein, A. F., Liu, C., Ikeda, K., Bullock, R., Rasmussen, R. M., Holland, G. J., & Clark, M. (2017). Simulating North American mesoscale convective systems with a convection-permitting climate model. *Climate Dynamics*, *55*(1–2), 95–110. https://doi.org/10.1007/s00382-017-3993-2

Prein, A. F., Rasmussen, R. M., Wang, D., & Giangrande, S. E. (2021). Sensitivity of organized convective storms to model grid spacing in current and future climates. *Philosophical Transactions of the Royal Society A*, *379*(2195), 20190546. https://doi.org/10.1098/rsta.2019.0546

Rackow, T., Pedruzo-Bagazgoitia, X., Becker, T., Milinski, S., Sandu, I., Aguridan, R., et al. (2024). Multi-year simulations at kilometre scale with the Integrated Forecasting System coupled to FESOM2. 5/NEMOv3. 4. *EGUsphere*, *2024*, 1–59. https://doi.org/10.5194/egusphere-2024-913

Roca, R., Aublanc, J., Chambon, P., Fiolleau, T., & Viltard, N. (2014). Robust observational quantification of the contribution of mesoscale convective systems to rainfall in the tropics. *Journal of Climate*, *27*(13), 4952–4958. https://doi.org/10.1175/JCLI-D-13-00628.1

Rodwell, M. J., Magnusson, L., Bauer, P., Bechtold, P., Bonavita, M., Cardinali, C., et al., (2013). Characteristics of occasional poor medium-range weather forecasts for Europe. *Bulletin of the American Meteorological Society*, *94*(9), 1393–1405. https://doi.org/10.1175/BAMS-D-12-00099.1

Rotunno, R., Klemp, J. B., & Weisman, M. L. (1988). A theory for strong, long-lived squall lines. *Journal of the Atmospheric Sciences*, *45*(3), 463–485. https://doi.org/10.1175/1520-0469_1988_045_0463_atfsll_2_0_co_2.xml

Schumacher, C., & Houze, R. A. (2003). Stratiform rain in the tropics as seen by the TRMM precipitation radar. *Journal of Climate*, *16*(11), 1739–1756. https://doi.org/10.1175/1520-0442(2003)016⟨1739:SRITTA⟩2.0.CO;2

Schumacher, C., Houze, R. A., & Kraucunas, I. (2004). The tropical dynamical response to latent heating estimates derived from the TRMM precipitation radar. *Journal of the Atmospheric Sciences*, *61*(12), 1341–1358. https://doi.org/10.1175/1520-0469(2004)061⟨1341:TTDRTL⟩2.0.CO;2

Schumacher, R. S., & Rasmussen, K. L. (2020). The formation, character and changing nature of mesoscale convective systems. *Nature Reviews Earth and Environment*, *1*(6), 300–314. https://doi.org/10.1038/s43017-020-0057-7

Segura, H., Hohenegger, C., Wengel, C., & Stevens, B. (2022). Learning by Doing: Seasonal and Diurnal Features of Tropical Precipitation in a Global–Coupled Storm–Resolving model. *Geophysical Research Letters*, *49*(24), e2022GL101796. https://doi.org/10.1029/2022GL101796

Senior, C. A., Marsham, J. H., Berthou, S., Burgin, L. E., Folwell, S. S., Kendon, E. J., et al. (2021). Convection permitting regional climate change simulations for understanding future climate and informing decision making in Africa. *Bulletin of the American Meteorological Society*, *102*(6), 1–46. https://doi.org/10.1175/BAMS-D-20-0020.1

Slingo, J., Bates, P., Bauer, P., Belcher, S., Palmer, T., Stephens, G., et al. (2022). Ambitious partnership needed for reliable climate prediction. *Nature Climate Change*, *12*(6), 499–503. https://doi.org/10.1038/s41558-022-01384-8

Smith, R. N. B. (1990). A scheme for predicting layer clouds and their water content in a general circulation model. *Quarterly Journal of the Royal Meteorological Society*, *116*(492), 435–460. https://doi.org/10.1002/qj.49711649210

Stevens, B., Adami, S., Ali, T., Anzt, H., Aslan, Z., Attinger, S., et al., (2023). Earth Virtualization Engines (EVE). *Earth System Science Data Discussions [preprint]*, *2023*, 1–14. https://doi.org/10.5194/essd-2023-376

Stevens, B., Satoh, M., Auger, L., Biercamp, J., Bretherton, C. S., Chen, X., et al., (2019). DYAMOND: The DYnamics of the Atmospheric general circulation Modeled On Non-hydrostatic Domains. *Progress in Earth and Planetary Science*, *6*(1), 1–17. https://doi.org/10.1186/s40645-019-0304-z

Stratton, R. A., Senior, C. A., Vosper, S. B., Folwell, S. S., Boutle, I. A., Earnshaw, P. D., et al. (2018). A Pan–African Convection-Permitting Regional Climate Simulation with the Met Office Unified Model: CP4-Africa. *Journal of Climate*, *31*(9), 3485–3508. https://doi.org/10.1175/JCLI-D-17-0503.1

Taylor, C. M., Belušić, D., Guichard, F., Parker, D. J., Vischel, T., Bock, O., et al. (2017). Frequency of extreme Sahelian storms tripled since 1982 in satellite observations. *Nature*, *544*(7651), 475–478. https://doi.org/10.1038/nature22069

Tomassini, L., Parker, D. J., Stirling, A., Bain, C., Senior, C., & Milton, S. (2017). The interaction between moist diabatic processes and the atmospheric circulation in African Easterly Wave propagation. *Quarterly Journal of the Royal Meteorological Society*, *143*(709), 3207–3227. https://doi.org/10.1002/qj.3173

Tomassini, L., Willett, M., Sellar, A., Lock, A., Walters, D., Whitall, M., et al., (2023). Confronting the convective gray zone in the global configuration of the Met Office Unified Model. *Journal of Advances in Modeling Earth Systems*, *15*(5), e2022MS003418. https://doi.org/10.1029/2022MS003418

Tomassini, L., & Yang, G.-Y. (2022). Tropical moist convection as an important driver of Atlantic Hadley circulation variability. *Quarterly Journal of the Royal Meteorological Society*, *148*(748), 3287–3302. https://doi.org/10.1002/qj.4359

Van Weverberg, K., Morcrette, C. J., Boutle, I., Furtado, K., & Field, P. R. (2021). A bimodal diagnostic cloud fraction parameterization. Part I: Motivating analysis and scheme description. *Monthly Weather Review*, *149*(3), 841–857. https://doi.org/10.1175/MWR-D-20-0224.1

Walters, D., Baran, A. J., Boutle, I., Brooks, M., Earnshaw, P., Edwards, J., et al. (2019). The Met Office Unified Model global atmosphere 7.0/7.1 and JULES global land 7.0 configurations. *Geoscientific Model Development*, *12*(5), 1909–1963. https://doi.org/10.5194/gmd-12-1909-2019

Wilson, D. R., & Ballard, S. P. (1999). A microphysically based precipitation scheme for the UK Meteorological Office Unified Model. *Quarterly Journal of the Royal Meteorological Society*, *125*(557), 1607–1636. https://doi.org/10.1002/qj.49712555707

Wilson, D. R., Bushell, A. C., Kerr-Munslow, A. M., Price, J. D., & Morcrette, C. J. (2008). PC2: A prognostic cloud fraction and condensation scheme. I: Scheme description. *Quarterly Journal of the Royal Meteorological Society*, *134*(637), 2093–2107. https://doi.org/10.1002/qj.333

Yang, G.-Y., & Slingo, J. (2001). The diurnal cycle in the tropics. *Monthly Weather Review*, *129*(4), 784–801. https://doi.org/10.1175/1520-0493(2001)129⟨0784:TDCITT⟩2.0.CO;2